Capability of the proposed long-baseline experiments to probe large extra dimension

Samiran Roy*

INFN—Sezione di Napoli, Complesso Universitario di Monte S. Angelo, I-80126 Napoli, Italy

(Received 29 May 2023; accepted 29 August 2023; published 14 September 2023)

Future long-baseline experiments will play an important role in exploring physics beyond the standard model. One such new physics concept is the large extra dimension (LED), which provides an elegant solution to the hierarchy problem. This model also explains the small neutrino mass in a natural way. The presence of the LED modifies the standard neutrino oscillation probabilities. Hence, the long-baseline experiments are sensitive to the LED parameters. We explore the potential of the three future long-baseline neutrino experiments, namely, T2HK, ESSnuSB, and DUNE, to probe the LED parameter space. We also compare the capability of the charged and neutral current measurements at DUNE to constrain the LED model. We find that T2HK will provide more stringent bounds on the largest compactification radius (R_{ED}) compared to the DUNE and ESSnuSB experiments. At 90% confidence limits, T2HK can exclude $R_{\mathrm{ED}} \sim 0.45\,(0.425)$ μm for the normal (inverted) mass hierarchy scenario.

DOI: 10.1103/PhysRevD.108.055015

I. INTRODUCTION

Neutrino oscillation firmly establishes the massive nature of neutrinos. The flavor and mass basis are not the same. They are related by a unitary mixing matrix which depends on three mixing angles (θ_{12}, θ_{13}, θ_{23}) and one CP-violating phase (δ_{cp}). The bound on the absolute mass of the neutrino coming from cosmology [1] and direct detection experiment [2] is an order of subelectronvolt. The smallness of neutrino mass compared to other standard model (SM) particles remains a puzzle to the scientific community. There are many promising theories beyond the standard model (BSM) that generate the small neutrino mass naturally. The inclusion of heavy right-handed neutrinos produces the small neutrino masses via a seesaw mechanism [3,4]. Another interesting mechanism that explains the small neutrino mass is the large extra dimension (LED) [5–7] which was first introduced to solve the hierarchy problems, i.e., the large discrepancy between the electroweak scale ($M_{\mathrm{EW}} \sim 10^3$ GeV) and the Plank scale ($M_{\mathrm{Pl}} \sim 10^{19}$ GeV) where the interaction of gravity becomes strong. In this model, the main assumption is that there exists only one fundamental scale which is the electroweak scale and in higher dimensions $(4+n)$ the two scales become equivalent, i.e., $M_{\mathrm{Pl}} \sim M_{\mathrm{EW}}$. But in four-dimensional space the value of M_{Pl} is large compared to M_{EW}. The inclusion of n compactified dimensions also modifies the inverse square law at a distance $10^{30/n-17}(\mathrm{TeV}/M_{\mathrm{EW}})^{(1+2/n)}$ cm [5]. One extra compactified dimension ($n=1$) case is ruled out from the observation of the verified gravitational inverse square law at solar scale, while the $n \geq 2$ scenario is allowed. Here, we consider an asymmetric space. Only one extra spatial dimension is large out of n compactified dimensions, and the space is effectively five dimensional. In this model, all the SM particles are confined to the four-dimensional brane which is a subspace of the full space-time. However, the SM singlet right-handed neutrino could propagate in more than four dimensions, and the large volume of extra dimensions provides suppression to the field in the four-dimensional space. This makes the mass of a neutrino very small [8–12] compared to other SM particles in a natural way.

The next-generation long-baseline experiments will play an important role in measuring the oscillation parameters with percentage-level precision. We consider three future long-baseline experiments, namely, T2HK [13–15], DUNE [16,17], and ESSnuSB [18–20]. The primary goal of these experiments is to address issues like mass hierarchy ($\Delta m^2_{31} > 0$ normal ordering, $\Delta m^2_{31} < 0$ inverted ordering), the octant of atmospheric mixing angle (θ_{23}), the determination of the value of δ_{cp}, etc. These experiments are also sensitive to physics beyond the standard three-neutrino oscillation framework. The presence of the LED modifies the neutrino oscillation. The departure from the standard oscillations can be parametrized by the Dirac mass of the lightest neutrino (m_0) and the radius of the largest compactified dimension (R_{ED}). Various neutrino experiments explore the LED model such as MINOS [21–23],

*samroy@na.infn.it

IceCube [24], beta decay experiments [25,26], reactor neutrino experiments [27,28], short-baseline experiments [29,30], JUNO [31], COHERENT measurements [32], etc. In this paper, we predict the bound on LED parameter space using the proposed experiments T2HK, ESSnuSB, and DUNE.

The paper is organized as follows: In Sec. II, we show the effect of the LED in the Lagrangian level, then we diagonalize the mass matrix and provide the expression of the neutrino oscillation probabilities in vacuum and the expression of the neutrino evolution in the presence of matter potential. Section III provides the simulation details of various experiments. Section IV contains the probability, event, and sensitivity analysis. Finally, we conclude in Sec. V.

II. FORMALISM

In the LED model, SM particles are confined to four-dimensional space, while the SM singlet right-handed neutrinos propagate to all dimensions, including the extra dimension. We augment the SM sector with the three five-dimensional singlet fermions $\Psi^{\alpha}_{L,R}$ corresponding to three active neutrinos ν^{α}_{L}. From the four-dimensional point of view, these singlet fields can be expressed as a tower of Kaluza-Klein (KK) modes ($\Psi^{\alpha(n)}_{L,R}, n = -\infty...\infty$) after the compactification of the fifth dimension with a periodic boundary condition. The KK modes behave like a large number of sterile neutrinos. We redefine the fields that couple to SM neutrino as $\nu^{\alpha(0)}_{R} \equiv \Psi^{\alpha(0)}_{R}$ and $\nu^{\alpha(n)}_{L,R} \equiv (\Psi^{\alpha(n)}_{L,R} + \Psi^{\alpha(-n)}_{L,R})/\sqrt{2}$. In this basis, the mass term of the Lagrangian [33] after the electroweak symmetry breaking is given by

$$L_{\text{mass}} = m^{D}_{\alpha\beta}\left(\bar{\nu}^{\alpha(0)}_{R}\nu^{\beta}_{L} + \sqrt{2}\sum_{n=1}^{\infty}\bar{\nu}^{\alpha(n)}_{R}\nu^{\beta}_{L}\right) + \sum_{n=1}^{\infty}\frac{n}{R_{\text{ED}}}\bar{\nu}^{(n)}_{R}\nu^{(n)}_{L} + \text{H.c.}, \tag{1}$$

where m^D is the Dirac mass matrix, and R_{ED} represents the radius of the compactification. The diagonalization of the mass matrix can be achieved in two steps. We define two 3×3 matrices U and r that diagonalize m^D, i.e., $m^{D}_{\text{diag}} = r^{\dagger}m^{D}U = \text{diag}(m^{D}_{1}, m^{D}_{2}, m^{D}_{3})$ and

$$\nu^{\alpha}_{L} = U^{\alpha i}\nu'^{i(0)}_{L}, \tag{2}$$

$$\nu^{\alpha(n)}_{R} = r^{\alpha i}\nu'^{i(n)}_{R}, \qquad n = 0\ldots\infty, \tag{3}$$

$$\nu^{\alpha(n)}_{L} = r^{\alpha i}\nu'^{i(n)}_{L}, \qquad n = 1\ldots\infty. \tag{4}$$

In the pseudo mass eigenstates $\nu'^{i}_{L} = (\nu'^{i}, \nu'^{i(1)}, \nu'^{i(2)}, ...)^{T}_{L}$ and $\nu'^{i}_{R} = (\nu'^{i(0)}, \nu'^{i(1)}, \nu'^{i(2)}, ...)^{T}_{R}$, the mass term in Eq. (1) becomes

$$L_{\text{mass}} = \sum_{i=1}^{3}\bar{\nu}'^{i}_{R}M^{i}\nu'^{i}_{L} + \text{H.c.}, \tag{5}$$

where M_i is an infinite-dimensional matrix expressed as

$$M^{i} = \frac{1}{R_{\text{ED}}}\begin{pmatrix} m^{D}_{i}R_{\text{ED}} & 0 & 0 & 0 & \ldots \\ \sqrt{2}m^{D}_{i}R_{\text{ED}} & 1 & 0 & 0 & \ldots \\ \sqrt{2}m^{D}_{i}R_{\text{ED}} & 0 & 2 & 0 & \ldots \\ \vdots & \vdots & \vdots & \vdots & \ddots \end{pmatrix}. \tag{6}$$

The true mass basis can achieved via diagonalization of the infinite-dimensional matrix M^i. We consider two infinite-dimensional matrices (L and R) such that $R^{\dagger}_{i}M^{i}L_{i}$ is diagonal, and the actual mass basis is given by $\nu^{i}_{L} = L^{\dagger}\nu'^{i}_{L}$ and $\nu^{i}_{R} = R^{\dagger}\nu'^{i}_{R}$. Hence, we can write the flavor basis brane neutrino as

$$\nu^{\alpha}_{L} = \sum_{i=1}^{3}U^{\alpha i}\sum_{n=0}^{\infty}L^{0n}_{i}\nu^{i(n)}_{L}. \tag{7}$$

L can be determined by the diagonalization of the Hermitian matrix $M^{\dagger}M$ [8–11] and given by

$$(L^{0n}_{i})^{2} = \frac{2}{1 + \pi^{2}(m^{D}_{i}R_{\text{ED}})^{2} + (\lambda^{(n)}_{i})^{2}/(m^{D}_{i}R_{\text{ED}})^{2}}, \tag{8}$$

where $(\lambda^{(n)}_{i})^{2}$ represents the eigenvalues of the matrices $R^{2}_{\text{ED}}M^{\dagger}_{i}M_{i}$, which can be found from the following equation:

$$\lambda^{(n)}_{i} - \pi(m^{D}_{i}R_{\text{ED}})^{2}\cot(\pi\lambda^{(n)}_{i}) = 0. \tag{9}$$

The mass of $\nu^{i(n)}_{L}$ is $\lambda^{(n)}_{i}/R_{\text{ED}}$ and

$$L^{jn}_{i} = \frac{\sqrt{2}jm^{D}_{i}R_{\text{ED}}}{(\lambda^{(n)}_{i})^{2} - j^{2}}L^{0n}_{i}, \tag{10}$$

where $j = 1...\infty$ and $n = 0...\infty$. We are interested in the scenario where the effect of LED can be treated as a perturbation with respect to the standard oscillation. This implies that $m^{D}_{i}R_{\text{ED}} \ll 1$. With this assumption, we can write

$$\lambda_i^{(0)} = m_i^D R_{\rm ED}\left(1-\frac{\pi^2}{6}(m_i^D R_{\rm ED})^2+\cdots\right), \qquad \lambda_i^{(j)} = j+\frac{1}{j}(m_i^D R_{\rm ED})^2+\cdots,$$
$$L_i^{00} = 1-\frac{\pi^2}{6}(m_i^D R_{\rm ED})^2+\cdots, \qquad L_i^{0j} = \frac{\sqrt{2}m_i^D R_{\rm ED}}{j}+\cdots,$$
$$L_i^{j0} = -\frac{\sqrt{2}m_i^D R_{\rm ED}}{j}+\cdots, \qquad L_i^{jj} = 1-\frac{(m_i^D R_{\rm ED})^2}{j^2}+\cdots, \tag{11}$$

and $L^{kj} = \mathcal{O}((m_i^D R_{\rm ED})^2)$ for $k \neq j = 1 \times \cdots \infty$. The transition probability of a particular neutrino flavor ν_α to ν_β in the presence of the LED is given by

$$P_{\alpha\beta}(L,E) = \left|\sum_{i=1}^{3} U^{\alpha i}U^{*\beta i}A_i(L,E)\right|^2, \tag{12}$$

where L is the distance between the source and detector, E represents the energy of the neutrino, and

$$A_i(L,E) = \sum_{n=0}^{\infty}(L_i^{0n})^2 \exp\left(i\frac{\lambda_i^{(n)2}L}{2ER_{\rm ED}^2}\right). \tag{13}$$

Similarly, the active to sterile KK modes oscillation probability is

$$P_{\alpha s}(L,E) = \sum_{i=1}^{3}\sum_{j=1}^{\infty}|B_{\alpha i(j)}|^2, \tag{14}$$

where

$$B_{\alpha i(j)} = U^{\alpha i}\sum_{n=0}^{\infty}L_i^{0n}L^{jn}\exp\left(i\frac{\lambda_i^{(n)2}L}{2ER_{\rm ED}^2}\right). \tag{15}$$

The neutrino masses $(\lambda_i^{(0)}/R_{\rm ED})$ of the mostly active neutrinos and Dirac masses (m_i^D) are related by the first term of Eq. (11), and we can write $\Delta m_{ij}^2 R_{\rm ED}^2 = (\lambda_i^{(0)})^2 - (\lambda_j^{(0)})^2$. The known values of the solar (Δm_{21}^2) and atmospheric (Δm_{31}^2) mass squared difference can be utilized to remove two parameters (m_2^D, m_3^D) from the theory, and the oscillation probability depends only on the $m_1^D (\equiv m_0)$ and $R_{\rm ED}$ parameters.

The vacuum neutrino oscillation probability is modified in matter. In the presence of the LED, the time evolution of the neutrino is described by the following equation [34]:

$$i\frac{d}{dt}\nu'_{iL} = \left[\frac{1}{2E_\nu}M_i^\dagger M_i \nu'_{iL} + \sum_{j=1}^{3}\begin{pmatrix} V_{ij} & 0_{1\times n} \\ 0_{n\times 1} & 0_{n\times n}\end{pmatrix}\nu'_{iL}\right]_{n\to\infty},$$
$$V_{ij} = \sum_{\alpha=e,\mu,\tau}U_{\alpha i}^* U_{\alpha j}(\delta_{\alpha e}V_{\rm CC}+V_{\rm NC}), \tag{16}$$

where the $V_{CC} = \sqrt{2}G_F n_e$ and $V_{NC} = -1/\sqrt{2}G_F n_n$ are the charged and neutral current matter potential, respectively. n_e and n_n represent the number density of the electron and neutron, respectively. We consider the equal number density of the electron and neutron and keep the matter density constant throughout the neutrino evolution for different baselines. We assume two KK modes for our analysis, and the result remains unaffected by the inclusion of the higher number of modes.

III. SIMULATION DETAILS

T2HK: There is a plan to upgrade the Super-Kamiokande (SK) [35] program in Japan to Hyper-Kamiokande [13–15]. This involves a roughly 20-fold increase in the fiducial mass of SK. We consider two 187 kt third-generation water Cherenkov detectors that will be installed close to the existing SK site. The detector will also receive an intense beam of neutrinos from the J-PARC proton accelerator research complex in Tokai, Japan, which is placed 295 km away from the detector site. This setup is commonly known as T2HK. The proton beam power at the J-PARC facility is 1.3 MW, which will generate 27×10^{21} protons on target (POT) in a total run-time of ten years. We consider the 2.5° off-axis flux, and the run-time is divided in a 1:3 ratio in neutrino and antineutrino modes, i.e., 2.5 years for the neutrino run while 7.5 years for the antineutrino run. The signal normalization errors in the $\nu_e(\bar{\nu}_e)$ appearance and $\nu_\mu(\bar{\nu}_\mu)$ disappearance channels are 3.2% (3.6%) and 3.9% (3.6%), respectively. In this work, we consider the background and energy calibration errors to be 10% and 5%, respectively, for all channels.

ESSnuSB: ESSnuSB [18–20] is a proposed water Cherenkov detector with a fiducial mass of 538 kt. There are two possible baseline configurations for the setup: either at 540 km or at 360 km away from the source. The European Spallation Source will produce an intense neutrino flux by hitting 2.7×10^{23} protons on target per year. The kinetic energy of the proton is 2.5 GeV. We consider overall 5% signal and 10% background normalization errors both in the appearance and disappearance channels for the neutrino and antineutrino runs. The ten years of run-time are equally divided between the neutrino and antineutrino modes. We consider the same setup configuration for both baselines in our analysis.

TABLE I. Benchmark value and its marginalization range for the standard neutrino oscillation parameters for the normal and inverted hierarchy scenarios. These values are compatible with the global fit of the oscillation parameters [42–44].

Parameter	Normal hierarchy	Inverted hierarchy
$\sin^2\theta_{12}$	0.304 ± 0.012	0.304 ± 0.012
$\sin^2\theta_{13}$	0.02219 ± 0.00062	0.02219 ± 0.00062
$\sin^2\theta_{23}$	0.5 ± 0.086	0.5 ± 0.086
Δm^2_{21}	$(7.42 \pm 0.02) \times 10^{-5}$ eV^2	$(7.42 \pm 0.02) \times 10^{-5}$ eV^2
Δm^2_{31}	$(2.517 \pm 0.028) \times 10^{-3}$ eV^2	$-(2.498 \pm 0.028) \times 10^{-3}$ eV^2
δ_{cp}	$-\pi/2[-\pi:\pi]$	$-\pi/2[-\pi:\pi]$

DUNE: DUNE [16,17] is an upcoming superbeam long-baseline (1300 km) neutrino experiment at Fermilab, USA, capable of determining the present unknowns of the neutrino oscillation parameters. The optimized beam of 1.07 MW–80 GeV protons at Fermilab will provide 1.47×10^{21} POT per year. We consider a 40 kt liquid argon detector and a total of seven years of run-time, which is equally divided between neutrino and antineutrino runs. All the experimental details are taken from [36]. We consider both the charged and neutral current measurements in our analysis. The detailed information for the neutral current (NC) events is taken from [37]. The detection efficiency of the NC event is assumed to be 90%. In a NC process, the outgoing neutrino also takes away some fraction of the incoming neutrino energy. Because of this, the reconstructed energy is typically lower than the total incoming energy, and a Gaussian energy resolution function cannot provide the correct events spectra. We use migration matrices [38] to simulate the NC events spectra appropriately. Moreover, we also take 10% of the charged current (CC) events as NC background, both in the neutrino and antineutrino modes. The normalization errors for the signal

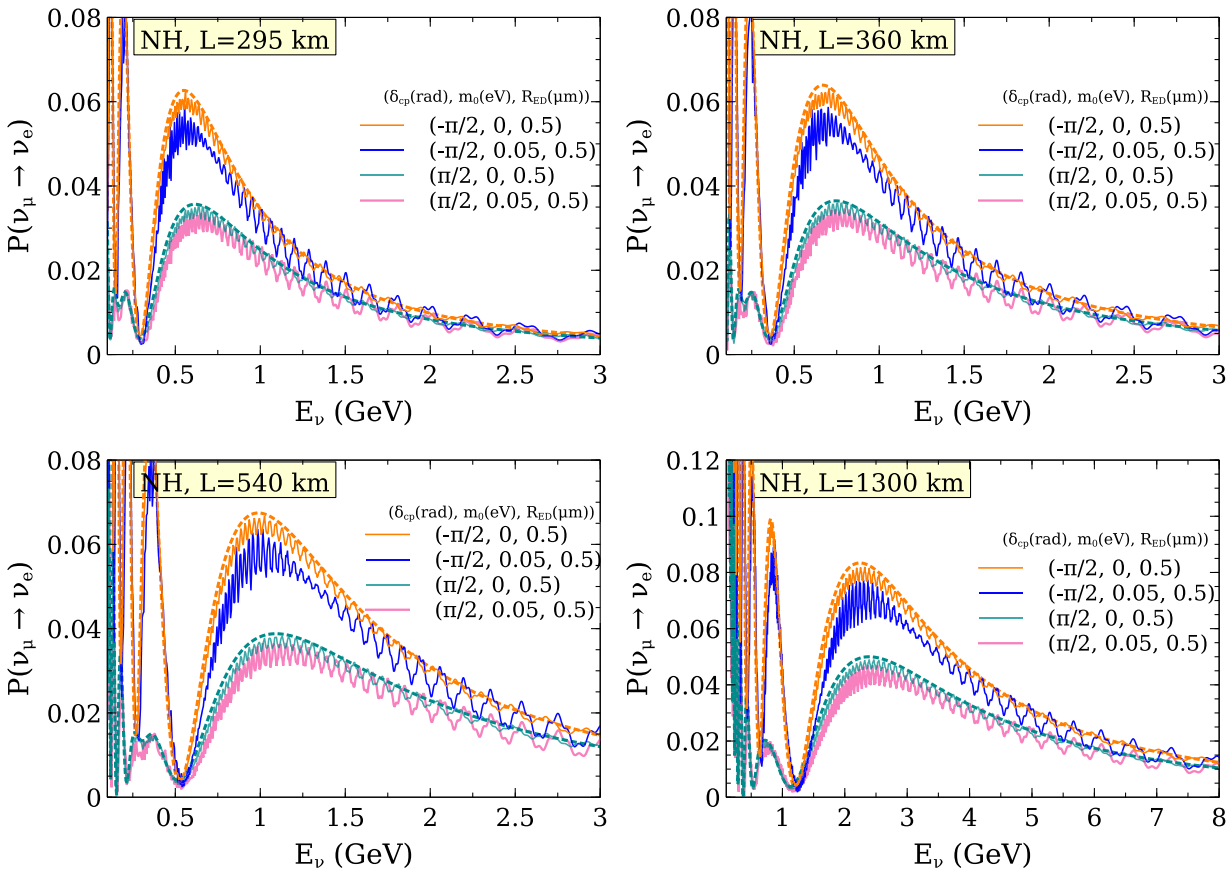

FIG. 1. Appearance oscillation probabilities in the presence of the LED for two values of *CP* phases and baselines. The dotted line corresponds to the standard oscillation scenario.

and background are assumed to be 5% and 10%, respectively. All other pertinent details regarding the NC analysis are taken from [39].

We use GLoBES software [40,41] to simulate the events in various detectors. The effect of the LED is included by changing the probability engine. We consider the constant matter density (2.95 gm/cc) for our simulation purposes. The values of the standard oscillation parameters and their marginalization ranges are given in Table I. We use the central values of the oscillation parameters for the probability, event, and sensitivity predictions in the next section.

IV. RESULTS

In Fig. 1, we show the neutrino appearance oscillation probabilities for different baselines, i.e., T2HK (295 km), ESSnuSB (360 km), ESSnuSB (540 km), and DUNE (1300 km). The dotted line corresponds to the standard neutrino oscillation for the two choices of δ_{cp} ($-\pi/2$ and $\pi/2$), while the solid line represents the probability with the LED model for two combinations of (m_0, R_{ED}) parameters for a given value of *CP* phase. We can observe from the plot that the oscillation probability increases with the increase in baseline length due to the increasing matter effect and the first oscillation maxima shifting toward higher neutrino energies. In the presence of the LED, the oscillation probabilities decrease from the standard prediction, and a wiggle appears due to the fast oscillation in the KK modes. The oscillation pattern remains almost similar for all the baselines. The effect of the LED increases with the increase of the lightest Dirac mass for a particular value of R_{ED}. This is also evident from Eqs. (11) and (12). In Fig. 2, we show the disappearance probability for different baselines for the standard (dotted lines) as well as LED cases (solid lines). We show the plot only for one value of the *CP* phase ($\delta_{cp} = 0$), as the effect of the *CP* phase is mild in the disappearance channel, and all other values of the *CP* phase give almost similar probabilities. The deviation from the standard oscillation due to the LED becomes larger with higher incoming neutrino energy beyond the first oscillation maxima point. Hence, if the neutrino fluxes peak at a higher energy than the first oscillation maxima, then the effect of the LED will be greater. The appearance and disappearance events for the neutrino run are shown in Figs. 3 and 4, respectively. For T2HK and DUNE, the maximum number of

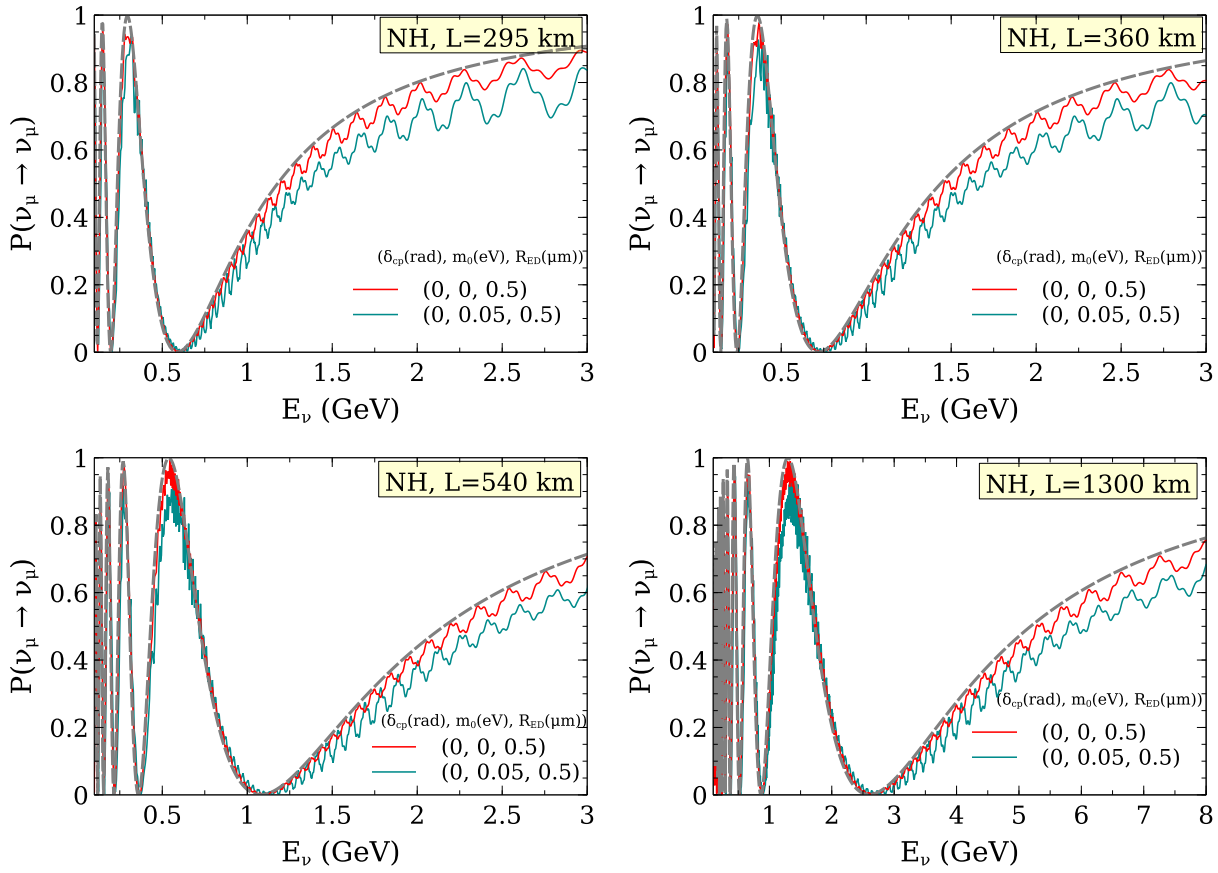

FIG. 2. Disappearance oscillation probabilities in the presence of the LED for different baselines and LED parameters. We choose the value of δ_{cp} to be 0, and all other *CP* phases will give almost similar probabilities as the dependence of the *CP* phase on the disappearance channel is mild. The dotted line corresponds to the standard scenario.

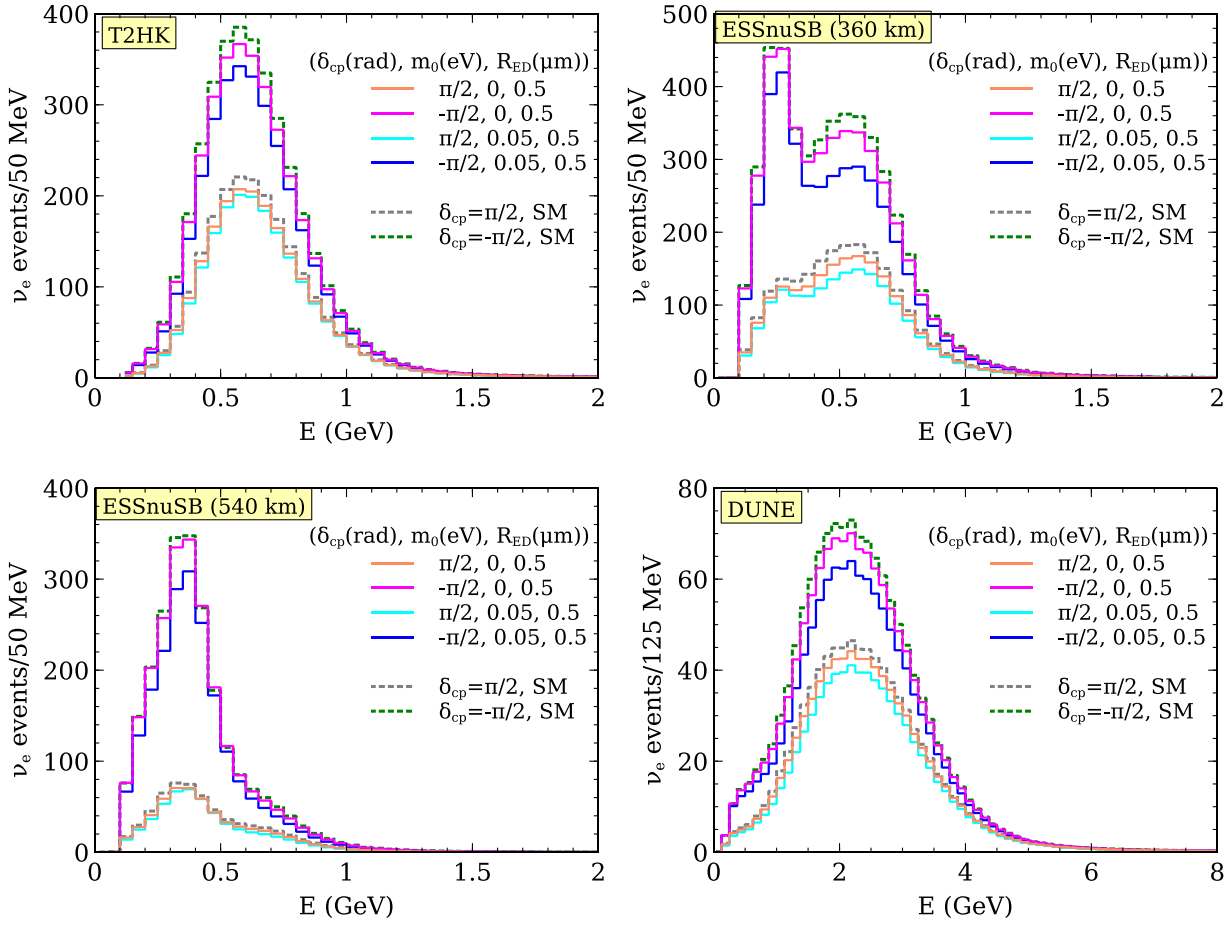

FIG. 3. Appearance events in the T2HK, ESSnuSB, and DUNE detectors for the standard (dotted lines) as well as the LED case (solid lines) for various values of *CP* phase.

appearance events occurs where both the first oscillation maxima and the peak of the fluxes coincide. But that is not the case for the ESSnuSB detector at 540 km. The second oscillation maxima and peak of the fluxes appear at ∼0.3 GeV, and there are almost negligible fluxes beyond 1 GeV. Also, for the ESSnuSB detector at 360 km, the peak of the flux and the first oscillation maxima do not coincide. We can observe from the plot that the standard and LED cases ν_e events change significantly with the change of δ_{cp} values. In the disappearance channel, we only show the $\delta_{cp} = 0$ case, as the dependence of events on the *CP* phase is very small. The deviation of the events from the standard scenario is greater for T2HK and DUNE, where there are sufficient fluxes beyond the first oscillation maxima. For the ESSnuSB detector, most of the events are concentrated around 0.5 GeV, and there are almost negligible events beyond 1 GeV. The number of events decreases from the standard prediction in the presence of the LED, both in the appearance and disappearance channels. To quantify the effects of the LED parameters on standard oscillation, we perform the χ^2 analysis next.

The Poissonian χ^2 is defined as [45]

$$\chi^2 = \min_{\vec{\lambda},\alpha,\beta}\left[\sum_{i=1}^{n} 2\left(N_i^{\text{test}} - N_i^{\text{true}} + N_i^{\text{true}} ln\frac{N_i^{\text{true}}}{N_i^{\text{test}}}\right) + \left(\frac{\alpha}{\sigma_s}\right)^2 + \left(\frac{\beta}{\sigma_b}\right)^2\right], \tag{17}$$

where $\vec{\lambda} = \{\theta_{12}, \theta_{13}, \theta_{23}, \Delta m^2_{21}, \Delta m^2_{31}, \delta_{cp}\}$, and α, β are two nuisance parameters. σ_s and σ_b represent the signal and background normalization errors, respectively. N_i^{test} and N_i^{true} are the test and true datasets in the ith energy bin. N_i^{true} can be expressed as

$$N_i^{\text{true}} = s_i(\vec{\lambda})(1+\alpha) + b_i(\vec{\lambda})(1+\beta), \tag{18}$$

where s_i and b_i represent the signal and background events in the ith energy bin. $N_i^{\text{test}} = s_i(\vec{\lambda}, m_0, R_{\text{ED}}) + b_i(\vec{\lambda}, m_0, R_{\text{ED}})$. We generate the true dataset using the standard oscillation scenario with the central values of the oscillation parameters as in Table I. In the test datasets, we

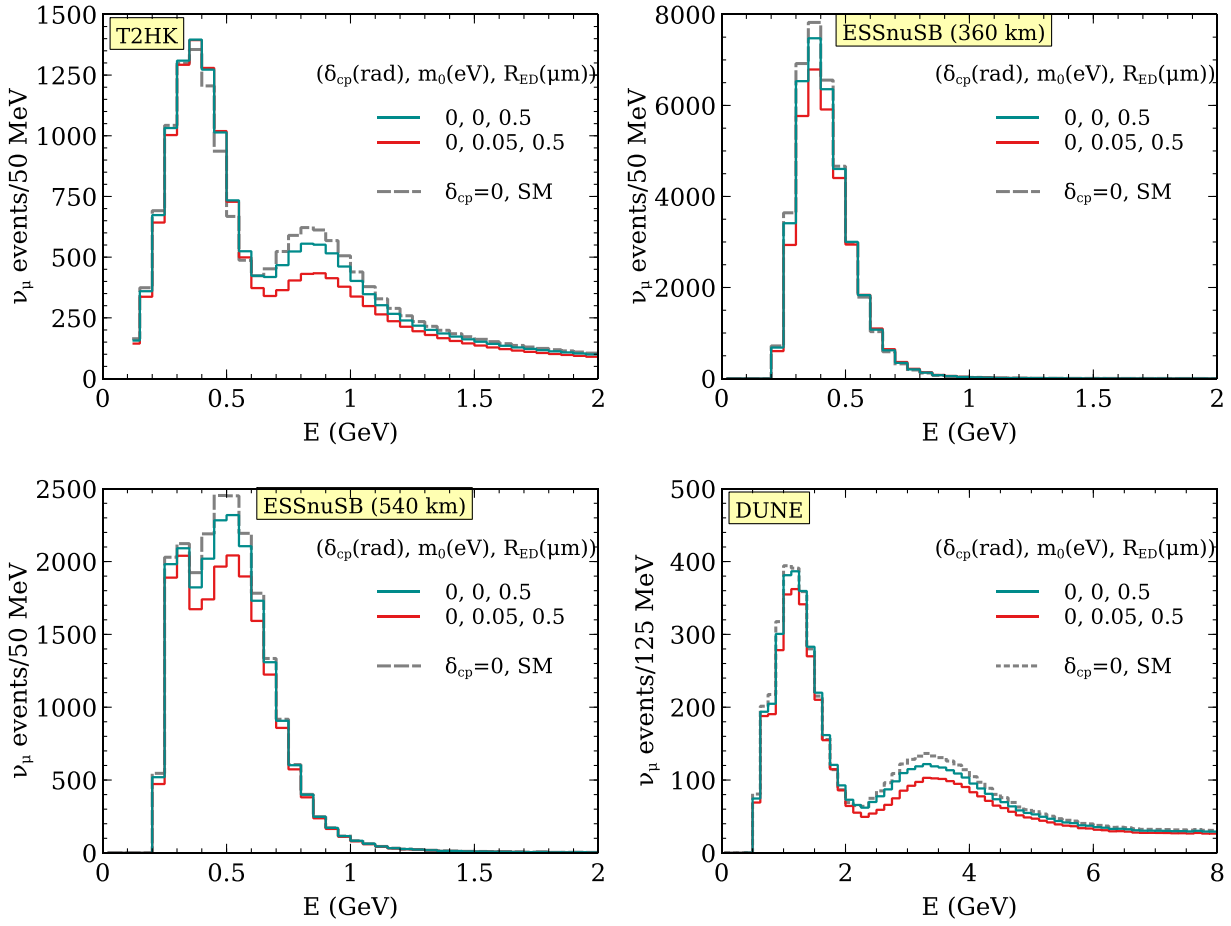

FIG. 4. Disappearance events in the T2HK, ESSnuSB, and DUNE detectors for the standard (dotted lines) as well as the LED case (solid lines) for $\delta_{cp} = 0$.

consider the LED model and marginalize the χ^2 over both the oscillation parameter uncertainties and systematic uncertainties, and report the minimum χ^2.

The bounds on LED parameters at 90% confidence limits (C.L.) ($\Delta\chi^2 = 4.61$, 2 degrees of freedom) in the $R_{\rm ED} - m_0$ plane are shown in Fig. 5. The left and right panels correspond to the normal and inverted hierarchy scenarios, respectively. Regions toward the right (left) of the curve are excluded (allowed) at 90% C.L. from the respective experiments. We can observe from the figure that

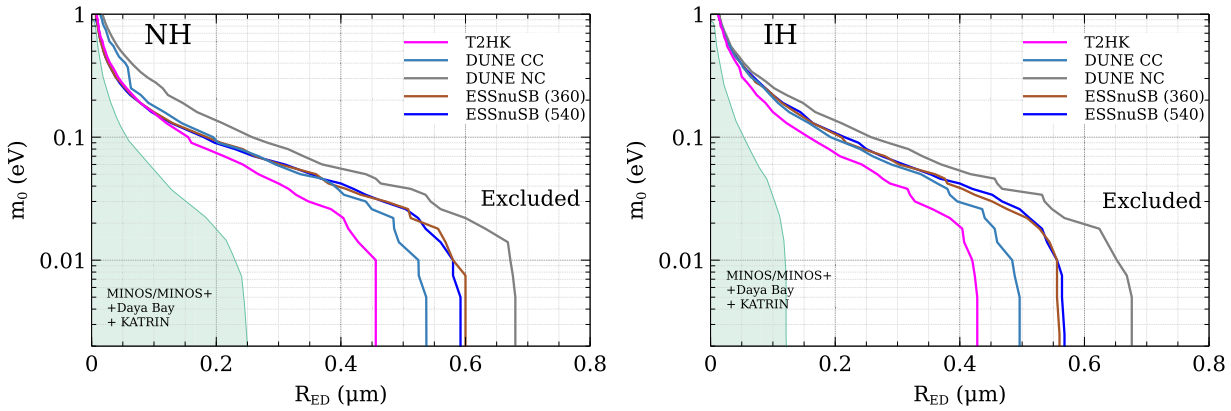

FIG. 5. The constraints on LED parameters in the $R_{\rm ED} - m_0$ plane at 90% C.L. ($\Delta\chi^2 = 4.61$) for the normal (left panel) and inverted (right panel) hierarchy scenarios. The green shaded region represents the constraint coming from the combined analysis of MINOS/MINOS+, Daya Bay, and KATRIN [23].

T2HK will be able to provide the best bound on the LED parameters, and at 90% C.L., it can exclude the value of $R_{\mathrm{ED}} > 0.45$ μm ($R_{\mathrm{ED}} > 0.425$ μm) for the normal hierarchy (NH) [inverted hierarchy (IH)] scenario. The better constraint in T2HK is attributed to the higher statistics compared to all other experiments. This is also seen from the event plots in Figs. 3 and 4. With the increase in mass m_0, the constraint on R_{ED} becomes more stringent. At $m_0 = 1$ eV, all the experiments can rule out $R_{\mathrm{ED}} \gtrsim 0.02$ μm. The constraint on the extra dimension using the charged current measurements is shown by the cyan line for DUNE. These results are consistent with [34,46]. Here, we also explore the capabilities of neutral current measurements. The NC events depend on the total number of active flavors present in the neutrino beam. Because of the oscillation in KK sterile modes, the total number of active flavors drops from unity depending on the values of m_0 and R_{ED}. We can see from Fig. 5 that the NC measurements provide much weaker constraints compared to the CC measurements. We can understand this from Eqs. (14) and (15). Because of the presence of L^{jn} terms, the dependence of NC probabilities on m_0 and R_{ED} is much weaker than CC oscillation probabilities. We also checked that the combination of CC and NC did not improve the results further. The two baseline configurations of ESSnuSB will provide almost similar bounds on the LED parameters for the NH and IH scenarios. ESSnuSB can rule out the $R_{\mathrm{ED}} > 0.60$ μm ($R_{\mathrm{ED}} > 0.55$ μm) for the NH (IH) scenario. The present constraint on the LED model coming from MINOS is $R_{\mathrm{ED}} > 0.7$ μm [22] for a very small mass of m_0 in the NH scenario. MINOS/MINOS+ and Daya Bay [23] rule out $R_{\mathrm{ED}} > 0.25(0.29)$ μm and $R_{\mathrm{ED}} > 0.65(0.12)$ μm, respectively, for NH (IH). For MINOS (MINOS+), the fluxes peaked at 3 GeV (7 GeV), while the first oscillation maxima was at 1.4 GeV. We observe from the disappearance plot that the deviation from the standard prediction increases for larger neutrino energies beyond the first oscillation maxima point. Because of the availability of higher energy fluxes, the constraint coming from MINOS (MINOS+) is more stringent than T2HK, DUNE, and ESSnuSB. The Daya Bay experiment is capable of putting a strong bound on LED parameters for IH compared to NH as the $\bar{\nu}_e$ disappearance channel is affected more by LED parameters in the IH scenario. The absolute mass of the neutrino is constrained by the KATRIN experiment. Hence, the combined experiments (MINOS/MINOS+, Daya Bay, and KATRIN) provide strong constraints on the LED parameters [23] as shown by the green shaded region in Fig. 5. IceCube data exclude $R_{\mathrm{ED}} > 0.4$ μm [24] at 2σ C.L. The future long-baseline experiments T2HK, ESSnuSB, and DUNE will be able to test the LED model independently, and the constraints are comparable to the existing bounds on R_{ED} parameters. These bounds are 2 orders of magnitude stronger than the constraints coming from tabletop experiments, which put a bound on $R_{\mathrm{ED}} > 37$ μm [47] at 95% C.L.

V. CONCLUSIONS

The LED model provides an attractive solution to the hierarchy problem. It also explains the small neutrino mass in a natural way. In this model, all the SM fields are confined to four-dimensional space, and SM singlet right-handed neutrinos could propagate in more than four-dimensional space. The large volume of the extra dimension provides suppression of the coupling of right-handed neutrino to four-dimensional SM neutrino fields and generates small neutrino mass. We consider three five-dimensional right-handed neutrino fields. These fields behave as a tower of KK modes in four-dimensional space after the compactification of the fifth dimension. The oscillation probability depends on the value of the lightest Dirac mass (m_0) and the value of the compactification radius (R_{ED}). We investigate the capability of the proposed long-baseline experiments T2HK, ESSnuSB, and DUNE to explore the LED parameter space. We find that T2HK will provide the most stringent constraint on R_{ED} compared to ESSnuSB and DUNE. We show the capability of NC measurements to constrain the LED parameters at DUNE. The constraint coming from NC measurements is weaker compared to CC measurements. The combination of CC and NC will not improve the bounds further. The two baseline configurations of ESSnuSB are able to give almost similar constraints on R_{ED} for the NH and IH scenarios.

ACKNOWLEDGMENTS

We thank Monojit Ghosh for providing the GLoBES glb file for the ESSnuSB detector on behalf of the ESSnuSB Collaboration. This work was partially supported by the research Grant No. 2017W4HA7S "NAT-NET: Neutrino and Astroparticle Theory Network" under the program PRIN 2017 funded by the Italian Ministero dell'Università e della Ricerca (MUR).

[1] N. Aghanim *et al.* (Planck Collaboration), Astron. Astrophys. **641**, A6 (2020); **652**, C4(E) (2021).
[2] M. Aker *et al.* (KATRIN Collaboration), Nat. Phys. **18**, 160 (2022).
[3] R. N. Mohapatra and G. Senjanović, Phys. Rev. Lett. **44**, 912 (1980).
[4] J. Schechter and J. W. F. Valle, Phys. Rev. D **22**, 2227 (1980).
[5] N. Arkani-Hamed, S. Dimopoulos, and G. R. Dvali, Phys. Lett. B **429**, 263 (1998).
[6] I. Antoniadis, N. Arkani-Hamed, S. Dimopoulos, and G. R. Dvali, Phys. Lett. B **436**, 257 (1998).
[7] N. Arkani-Hamed, S. Dimopoulos, and G. R. Dvali, Phys. Rev. D **59**, 086004 (1999).
[8] N. Arkani-Hamed, S. Dimopoulos, G. R. Dvali, and J. March-Russell, Phys. Rev. D **65**, 024032 (2001).
[9] K. R. Dienes, E. Dudas, and T. Gherghetta, Nucl. Phys. **B557**, 25 (1999).
[10] G. R. Dvali and A. Y. Smirnov, Nucl. Phys. **B563**, 63 (1999).
[11] R. Barbieri, P. Creminelli, and A. Strumia, Nucl. Phys. **B585**, 28 (2000).
[12] F. Nortier, Int. J. Mod. Phys. A **35**, 2050182 (2020).
[13] K. Abe *et al.* (Hyper-Kamiokande proto-Collaboration), Prog. Theor. Exp. Phys. **2015**, 053C02 (2015).
[14] K. Abe *et al.* (Hyper-Kamiokande Collaboration), Prog. Theor. Exp. Phys. **2018**, 063C01 (2018).
[15] K. Abe *et al.* (Hyper-Kamiokande Collaboration), arXiv:1805.04163.
[16] R. Acciarri *et al.* (DUNE Collaboration), arXiv:1512.06148.
[17] R. Acciarri *et al.* (DUNE Collaboration), arXiv:1601.02984.
[18] E. Baussan *et al.* (ESSnuSB Collaboration), Nucl. Phys. **B885**, 127 (2014).
[19] A. Alekou *et al.*, Eur. Phys. J. Spec. Top. **231**, 3779 (2022).
[20] M. Ghosh, J. Phys. Conf. Ser. **2156**, 012133 (2021).
[21] P. A. N. Machado, H. Nunokawa, and R. Zukanovich Funchal, Phys. Rev. D **84**, 013003 (2011).
[22] P. Adamson *et al.* (MINOS Collaboration), Phys. Rev. D **94**, 111101 (2016).
[23] D. V. Forero, C. Giunti, C. A. Ternes, and O. Tyagi, Phys. Rev. D **106**, 035027 (2022).
[24] A. Esmaili, O. L. G. Peres, and Z. Tabrizi, J. Cosmol. Astropart. Phys. 12 (2014) 002.
[25] V. S. Basto-Gonzalez, A. Esmaili, and O. L. G. Peres, Phys. Lett. B **718**, 1020 (2013).
[26] W. Rodejohann and H. Zhang, Phys. Lett. B **737**, 81 (2014).
[27] A. Di Iura, I. Girardi, and D. Meloni, J. Phys. G **42**, 065003 (2015).
[28] I. Girardi and D. Meloni, Phys. Rev. D **90**, 073011 (2014).
[29] M. Carena, Y.-Y. Li, C. S. Machado, P. A. N. Machado, and C. E. M. Wagner, Phys. Rev. D **96**, 095014 (2017).
[30] G. V. Stenico, D. V. Forero, and O. L. G. Peres, J. High Energy Phys. 11 (2018) 155.
[31] V. S. Basto-Gonzalez, D. V. Forero, C. Giunti, A. A. Quiroga, and C. A. Ternes, Phys. Rev. D **105**, 075023 (2022).
[32] A. N. Khan, J. High Energy Phys. 01 (2023) 052.
[33] H. Davoudiasl, P. Langacker, and M. Perelstein, Phys. Rev. D **65**, 105015 (2002).
[34] J. M. Berryman, A. de Gouvêa, K. J. Kelly, O. L. G. Peres, and Z. Tabrizi, Phys. Rev. D **94**, 033006 (2016).
[35] Y. Fukuda *et al.* (Super-Kamiokande Collaboration), Phys. Rev. Lett. **81**, 1562 (1998).
[36] T. Alion *et al.* (DUNE Collaboration), arXiv:1606.09550.
[37] C. Adams *et al.* (LBNE Collaboration), arXiv:1307.7335.
[38] V. De Romeri, E. Fernandez-Martinez, and M. Sorel, J. High Energy Phys. 09 (2016) 030.
[39] R. Gandhi, B. Kayser, S. Prakash, and S. Roy, J. High Energy Phys. 11 (2017) 202.
[40] P. Huber, M. Lindner, and W. Winter, Comput. Phys. Commun. **167**, 195 (2005).
[41] P. Huber, J. Kopp, M. Lindner, M. Rolinec, and W. Winter, Comput. Phys. Commun. **177**, 432 (2007).
[42] I. Esteban, M. C. Gonzalez-Garcia, M. Maltoni, T. Schwetz, and A. Zhou, J. High Energy Phys. 09 (2020) 178.
[43] F. Capozzi, E. Di Valentino, E. Lisi, A. Marrone, A. Melchiorri, and A. Palazzo, Phys. Rev. D **104**, 083031 (2021).
[44] P. F. de Salas, D. V. Forero, S. Gariazzo, P. Martínez-Miravé, O. Mena, C. A. Ternes, M. Tórtola, and J. W. F. Valle, J. High Energy Phys. 02 (2021) 071.
[45] P. Huber, M. Lindner, and W. Winter, Nucl. Phys. **B645**, 3 (2002).
[46] B. Abi *et al.* (DUNE Collaboration), Eur. Phys. J. C **81**, 322 (2021).
[47] P. A. Zyla *et al.* (Particle Data Group), Prog. Theor. Exp. Phys. **2020**, 083C01 (2020).